Catalysis Today 161 (2011) 196–201

Contents lists available at ScienceDirect

Catalysis Today

journal homepage: www.elsevier.com/locate/cattod

Photonic efficiency and mechanism of photocatalytic molecular hydrogen production over platinized titanium dioxide from aqueous methanol solutions

Tarek A. Kandiel[a], Ralf Dillert[a], Lars Robben[b], Detlef W. Bahnemann[a,*]

[a] Institut für Technische Chemie, Leibniz Universität Hannover, Callinstrasse 3, D-30167 Hannover, Germany
[b] Institut für Mineralogie, Leibniz Universität Hannover, Callinstrasse 3, D-30167 Hannover, Germany

ARTICLE INFO

Article history:
Available online 16 September 2010

Keywords:
Titanium dioxide
Photocatalytic H_2 production
Methanol
Sacrificial system
Water splitting

ABSTRACT

The photocatalytic molecular hydrogen (H_2) production from aqueous methanol solutions over Pt-loaded commercial (Evonik Aeroxide TiO_2 P25 and Sachtleben Hombikat UV100) and home made (TiO_2 P25HT) titanium dioxide photocatalysts has been studied. The photonic efficiencies were calculated by dividing the H_2 production rate by the photon flux. The effect of the employed light intensity on the H_2 production rate was investigated. The products of the photocatalytic methanol oxidation were quantitatively analyzed employing different test conditions, i.e., different illumination times, pH values, and methanol concentrations. The balance between the amount of evolved H_2 and the amount of photocatalytic methanol oxidation products was checked. Based on the obtained results, the difference in the photocatalytic activities between the investigated photocatalysts, the effect of the employed light intensities, and the description of the photocatalytic H_2 production from aqueous methanol solutions is discussed.

1. Introduction

Recently, growing environmental concern and an increasing energy demand are driving the search for new, sustainable sources of energy. In particular, solar molecular hydrogen (H_2) has attracted much attention because it can be regarded as a renewable and clean-burning energy source. Among the proposed technologies for its production, the photocatalytic conversion of biomass derived compounds is currently being discussed and investigated extensively [1,2]. Titanium dioxide is believed to be the most promising presently known photocatalyst, because of its superior photoreactivity, its nontoxicity, its long-term stability, and its low price; thus, many reports have been published concerning photocatalytic H_2 production activities [3–5].

Despite the fact that TiO_2 generally exhibits relatively high photocatalytic activity towards the degradation of organic compounds under UV illumination in the presence of molecular oxygen, it usually does not show any ability to photocatalyse the H_2 evolution in oxygen free systems even in the presence of an electron donor. When TiO_2 absorbs a photon the energy of which exceeds its bandgap energy, an electron (e^-)/hole (h^+) pair is generated. Both, e^- and h^+, can either migrate to the TiO_2 surface and react with adsorbed reactants in a photocatalytic process, or they may undergo an undesired recombination. In the presence of an electron donor, such as methanol, and in the absence of O_2, the excess holes will be consumed and the photogenerated electrons will be trapped near the surface forming tri-valent titanium (Ti^{3+}) sites instead of reducing H^+. This phenomenon has been observed by Bahnemann et al. [6] in laser-flash photolysis experiments employing suspensions of colloidal TiO_2. Loading the TiO_2 surface with small Pt islands creates sinks for the electrons thus facilitating the separation of e^-/h^+ pairs photogenerated in TiO_2 and promoting the formation of H_2 gas [7–11].

Methanol is frequently used as an electron donor in so-called "sacrificial systems" for the photocatalytic H_2 production; however, only a few mechanistic study of this system have been published [12,13]. Some reports describe the photocatalytic H_2 production from aqueous methanol solutions as water splitting [14–18], while other reports describe the process as dehydrogenation of methanol to formaldehyde or reforming of methanol to carbon dioxide [1,8]. Moreover, only little information exists concerning the photonic efficiency of this process and hardly any information concerning the effect of the light intensity on the rate of the photocatalytic H_2 evolution over Pt-loaded TiO_2 from aqueous methanol solution; however, this type of information is available for the photocatalytic oxidation of methanol in the presence of TiO_2 in aerated systems [8,19].

Hence, the photocatalytic H_2 production from aqueous methanol solutions over Pt-loaded commercial (Evonik Aeroxide TiO_2 P25 and Sachtleben Hombikat UV100) and home made (TiO_2 P25HT) titanium dioxide nanomaterials has been studied. The photonic efficiencies have been calculated. The effect of the

* Corresponding author. Tel.: +49 511 762 5560; fax: +49 511 762 2774.
E-mail address: bahnemann@iftc.uni-hannover.de (D.W. Bahnemann).

0920-5861/$ – see front matter © 2010 Elsevier B.V. All rights reserved.
doi:10.1016/j.cattod.2010.08.012

employed light intensity has been investigated. The products of the photocatalytic methanol oxidation have been qualitatively and quantitatively analyzed employing different test conditions, i.e., different illumination times, pH values, and methanol concentrations. In particular, the balance between the amount of evolved H_2 and the sum of the photocatalytic methanol oxidation products has been checked.

2. Experimental

2.1. Preparation and characterization of TiO_2 photocatalysts

TiO_2 anatase nanoparticles have been prepared by the hydrothermal treatment of TiO_2 P25 in alkaline solution. Typically, 1.0 g TiO_2 and 100 ml NaOH aqueous solution (10 M) were mixed and magnetically stirred for 2 h. The resulting suspension was poured into a Teflon-lined stainless steel autoclave (Berghof, DAB-3) and then heated in an electric furnace held at 120 °C for 24 h. The autoclave was allowed to naturally cool down to room temperature. The resulting white precipitate was vacuum filtrated and washed with HCl solution (0.1 M) and deionized water until neutrality (pH 7). The obtained precipitate was redispersed in HCl solution (0.5 M HCl) and stirred overnight followed by filtration and thorough washing with deionized water. The isolated powder was dried at 70 °C in an oven and post-heated in air atmosphere at 400 °C for 2 h (denoted TiO_2 P25HT). 0.5 wt% Pt-loaded TiO_2 photocatalysts have been prepared by a photochemical deposition method [20].

The bare and Pt-loaded TiO_2 photocatalysts have been characterized by X-ray diffraction (XRD), nitrogen adsorption and desorption isotherms, field emission-scanning electron microscopy (FE-SEM), and high-resolution transmission electron microscopy (HR-TEM). The details of the measurements have been described elsewhere [21,22].

2.2. Photocatalytic H_2 production test

The photocatalytic H_2 production tests have been performed in a double jacket Duran glass reactor (110 cm^3) with three outlets as described elsewhere [20]. A 10-cm water bath and a black bandpass filter (3 mm, UG1 SCHOTT glass) restricting the incident light to wavelengths between 300 and 400 nm were used during photon flux and photonic efficiencies measurements. The light intensity was adjusted by using neutral density filters (1.5 mm, LOT-ORIEL).

2.3. Analysis of the methanol photooxidation products

The amount of formaldehyde formed during the photooxidation of methanol has been determined by the Nash method [23] using a Varian Cary 100 spectrophotometer. The concentration of formic acid has been determined using a high performance DIONEX ICS-1000 ion chromatograph [20]. A Shimadzu gas chromatograph coupled with a mass spectrometer (GC-MS-QP 5000) has been used to detect any other intermediates and products.

3. Results

3.1. Photocatalysts characterization

The XRD diffraction patterns of TiO_2 P25 before and after hydrothermal treatment are shown in Fig. S1a and b, respectively (see supplementary data). A comparison of both XRD diffraction patterns clearly indicates that a phase transformation from the anatase and the rutile phases to the titanate ($H_2Ti_4O_9.H_2O$) structure occurs during the hydrothermal treatment. Calcination of the titanate at 400 °C for 2 h leads to the formation of the pure anatase phase as confirmed by the XRD measurement (see Fig. S1c) [24]. The BET surface area values and the Rietveld analysis of the XRD patterns for the investigated photocatalysts are given in Table S1 (see supplementary data). Interestingly, the BET surface area of the anatase nanoparticles (TiO_2 P25HT) is found to be 3.5 times larger than that of the starting material, i.e., TiO_2 P25. The Pt-loaded photocatalysts have also been characterized by X-ray diffraction and BET surface area measurements. The obtained diffraction patterns indicate that all the diffraction peaks of TiO_2 P25HT and of TiO_2 UV100 can be indexed to the anatase phase, whereas the rutile phase only exists in case of TiO_2 P25. No diffraction peaks are detected for Pt particles indicating that these are highly dispersed and very small particles. The quantitative phase composition and the crystallite diameters of Pt-loaded TiO_2 photocatalysts as evident from the Rietveld analysis of the XRD data as well as the BET surface areas are also given in Table S1. The results indicate that the BET surface area of TiO_2 P25HT, of TiO_2 P25, and of TiO_2 UV100 decreases following the Pt loading indicating that the Pt nanoparticles are deposited on the surface blocking some of the active sites for N_2 adsorption.

The morphologies of TiO_2 P25 before and after the hydrothermal treatment were investigated by FE-SEM. The obtained micrographs are shown in Fig. S2 (see supplementary data). It is obvious from the micrograph shown in Fig. S2a that TiO_2 P25 consists of secondary agglomerated particles formed from primary particles with an average particle size of about 25 nm. The micrograph shown in Fig. S2b also demonstrates that the hydrothermal treatment of TiO_2 P25 leads to the transformation from the spherical to a fiber like morphology. The subsequent calcination of this fiber like titanate material yields anatase nanoparticles exhibiting a rod like morphology. It seems that the fiber like particles are completely destroyed during the calcination step yielding small rods as confirmed by HR-TEM (see Fig. S3, supplementary data). The particle size of TiO_2 P25HT is found to be about 10 nm in good agreement with the crystallite size obtained from the XRD data analysis. The interesting point is that the hydrothermal treatment of TiO_2 P25 and the post heat treatment yields anatase nanoparticles with an average particle size that is about two times smaller than that of the starting material (TiO_2 P25).

3.2. Photocatalytic H_2 production

Fig. 1 shows the time courses of the photocatalytic H_2 evolution from aqueous methanol solution (0.03 M, 2.25 mmol methanol) over 0.5 wt% Pt-loaded TiO_2 photocatalysts, namely, TiO_2 P25, TiO_2 UV100, and TiO_2 P25HT. It is obvious from Fig. 1 that TiO_2 UV100 exhibits higher activity than TiO_2 P25 and even than TiO_2 P25HT. It is also obvious that bare TiO_2 photocatalysts without Pt loading do not exhibit photocatalytic H_2 evolution activity. No H_2 was evolved in the dark as well as under illumination in the absence of a photocatalysts.

The rate of the photocatalytic H_2 evolution is found to strongly depend on the methanol concentration initially present in the suspension (see supplementary data Fig. S4). It increases with increasing methanol concentration and then levels off to reach a plateau. Thus, a low methanol concentration (0.03 M, 2.25 mmol methanol) was employed during the photocatalytic experiment to avoid the high overpressure generated by the evolved H_2 at high methanol concentration allowing for longer reaction times in the sealed reactor. These experimental conditions also allow to investigate the possibility of water photooxidation in more detail. The photonic efficiency of the photocatalytic H_2 evolution was, however, calculated employing high methanol concentrations (4.93 M, 370 mmol methanol) in the plateau region of Fig. S4 in order to determine the maximum efficiency. No H_2 was detected

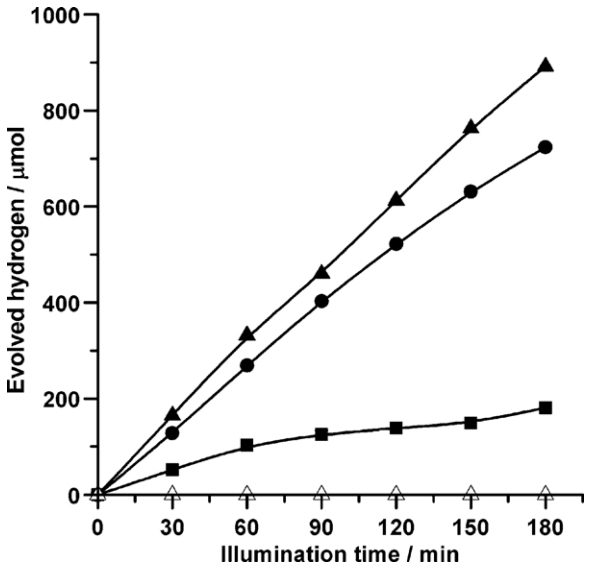

Fig. 1. Time course of the photocatalytic H_2 evolution over different 0.5 wt% Pt-loaded TiO_2 photocatalysts (■) TiO_2 P25, (●) TiO_2 P25HT, and (▲) TiO_2 UV100 and over bare TiO_2 photocatalysts without Pt loadings (△) TiO_2 UV100 (shown as example). Conditions: 0.5 g l^{-1} photocatalysts, 0.5 wt% Pt, 75 ml Ar-saturated aqueous methanol solution (0.03 M, 2.25 mmol methanol), UV(A)–Vis illumination (60 mW cm^{-2}), temperature (25 °C), natural pH (pH ≈6.5).

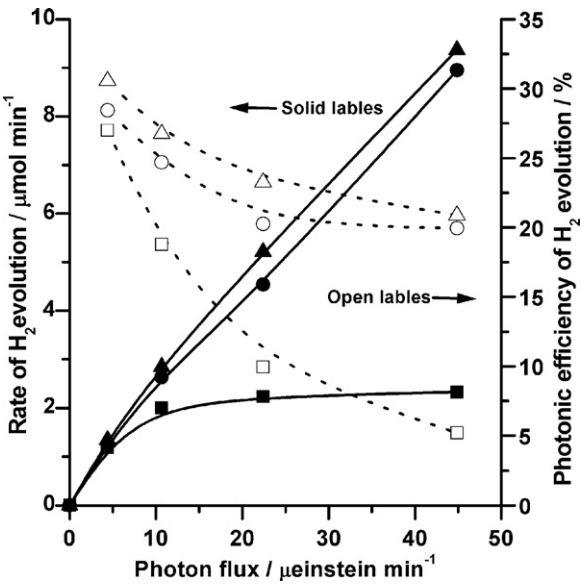

Fig. 2. Plot of the rate as well as the photonic efficiency of photocatalytic H_2 evolution over different 0.5 wt% Pt-loaded TiO_2 photocatalysts as a function of photon flux. (■, □) TiO_2 P25, (●, ○) TiO_2 P25HT, and (▲, △) TiO_2 UV100. Solid and open labels indicate the rate and the photonic efficiency, respectively. Conditions: 0.5 g l^{-1} photocatalysts, 0.5 wt% Pt, 75 ml Ar-saturated aqueous methanol solution (370 mmol methanol), UG1 black filter, UV(A) illumination (up to ≈45 μeinstein min^{-1}), temperature (25 °C), natural pH (pH ≈6.5).

in the absence of methanol, i.e., when pure water is employed [10,11].

To investigate the effect of the light intensity on the rate of the photocatalytic H_2 evolution, the latter were determined at different light intensities. The corresponding photonic efficiencies (ζ) have been calculated by dividing the H_2 production rate by the photon flux, I_0, which was determined under the same conditions using ferrioxalate actinometry [25,26]. Fig. 2 shows plots of the rate as well as the photonic efficiency as a function of the applied light flux. As shown in Fig. 2 a non-linear relation between the rate of H_2 evolution and the employed light flux was observed. The most interesting observation is that TiO_2 UV100 and TiO_2 P25HT, which both consist of pure phase anatase, exhibit the same behavior. They show a slight deviation from a linear dependence between the rate of the H_2 evolution and the light intensity at high light intensities. However, in case of TiO_2 P25, which is a mixture of rutile and anatase nanoparticles, the rate of photocatalytic H_2 evolution only increases initially with increasing light intensity quickly reaching a plateau of constant rate.

3.3. *Analysis of photocatalytic methanol oxidation products*

The balance between the amount of photocatalytic methanol oxidation products and the amount of H_2 gas evolved has been checked. The products were qualitatively and quantitatively analyzed following different illumination times and working at different pH values employing different methanol concentrations. In all experimental runs, formaldehyde, formic acid, and carbon dioxide were the only detected reaction products. The quantitative results of the analysis are listed in Table 1. They indicate that after 3 h of UV–Vis illumination of aqueous methanol solutions (0.03 M, 2250 μmol methanol) at different pH values (pH 3.0, 7.0, and 10) in the presence of Pt-loaded TiO_2 UV100, the amount of H_2 evolved is almost twice as high as the expected value calculated from the sum of all detected methanol photooxidation products (formaldehyde, formic acid, and carbon dioxide). To examine only the initial photooxidation step of methanol, the experiments were repeated at shorter UV–Vis illumination times (15 min) working again at different pH values (pH 3.0 and 7.0). Under these conditions, only formaldehyde was detected and its amount was found to be equimolar to the amount of H_2 evolved. The same results were obtained when the photooxidation products were measured at high methanol concentration (4.93 M, 3.7×10^5 μmol methanol, see Table 1).

Table 1
Quantitative analysis[a] of photocatalytic methanol oxidation products over 0.5 wt% Pt-loaded TiO_2 UV100 at different reaction times, pH values, and methanol concentrations.

Detected products (μmol)	Conditions: 2250 μmol methanol, 3 h UV(A)–Vis illumination			Conditions: 2250 μmol methanol, 15 min UV(A)–Vis illumination		Conditions: 3.7×10^5 μmol methanol, 15 min UV(A)–Vis illumination	
	pH			pH		pH	
	3.0	7.0	10.0	3.0	7.0	3.0	7.0
Molecular hydrogen	899	1118	946	62	80	260	290
Formaldehyde	285	323	283	59	75	286	323
Formic acid	7.54	7.84	25	–	–	–	–
Carbon dioxide	56	82	58	–	–	–	–
Calculated H_2	468	585	507	59	75	286	323

[a] The relative errors are less than 5% as judged from repeated measurements.

4. Discussion

4.1. The antenna mechanism

Pt-loaded TiO_2 UV100 exhibits higher photocatalytic activity for the H_2 evolution from aqueous methanol solution than Pt-loaded TiO_2 P25 and Pt-loaded TiO_2 P25HT, respectively (cf. Fig. 1). This higher photocatalytic activity of H_2 formation can be explained, at the first sight, by the fact that the surface area of TiO_2 UV100 is about six times larger than that of TiO_2 P25 and twice as large as that of TiO_2 P25HT (cf. Table S1). However, the observed differences in photocatalytic activity, in general, cannot be interpreted using only one single property of the photocatalysts [27]. In fact, the photocatalytic activity depends on various properties, e.g., surface area, crystallinity, particle size, optical properties, structure, nature of exposed crystal faces, charge recombination rate constants as well as upon many other factors. For example, the rates of the photocatalytic H_2 evolution over Pt-loaded TiO_2 UV100 and Pt-loaded TiO_2 P25HT were found to be 303 and 252 $\mu mol\,h^{-1}$, respectively, while their BET surface areas are 293 and 169 $m^2\,g^{-1}$, respectively. Though Pt-loaded TiO_2 UV100 has a significantly higher BET surface area than Pt-loaded TiO_2 P25HT, it does not exhibit a much higher photocatalytic activity.

On the other hand, the significantly higher photocatalytic activity of both, TiO_2 UV100 and TiO_2 P25HT, as compared with TiO_2 P25 can not only be explained by the fact that the latter has a lower BET surface area but also by the differences in structure and phase composition. TiO_2 UV100 and TiO_2 P25HT exhibit a mesoporous structure as proved by the N_2 adsorption–desorption isotherms (see supplementary data Figs. S5A and B, respectively), whereas TiO_2 P25 is completely non-porous (see supplementary data Fig. S5C). This mesoporous structure may either result from compactly packed nanoparticles or may be due to the agglomeration of the TiO_2 nanoparticles. This mesoporous structure can then provide suitable interfaces for facile interparticle charge transfer while the reactants can freely diffuse through the pores as illustrated in Fig. 3 [3,28]. While the excited TiO_2 nanoparticle can transfer the absorbed energy through the mesoporous TiO_2 network to other ground-state TiO_2 particles, the probability of the hole trapping at an hydroxyl surface group forming an adsorbed hydroxyl radical that is subsequently transferred to an adsorbed CH_3OH molecule is considered to be high. Consequently, the probability of electron transfer to the Pt particle is increased by an increased CH_3OH diffusion through the pores of the nanostructures. It is therefore suggested that the so-called antenna mechanism [22,29,30] together with an increased CH_3OH diffusion can be employed to explain the higher photocatalytic H_2 evolution over Pt-loaded TiO_2 UV100 and Pt-loaded TiO_2 P25HT. Within this antenna model, it can be imagined that the overlap of the energy bands of the TiO_2 nanoparticles forming this network will result in unified energy bands for the entire system enabling a quasi-free movement of the photogenerated charge carriers throughout the mesoporous structure. Consequently, an electron generated by light absorption within one of the nanoparticles forming the network will subsequently be available to promote redox processes anywhere within the structure.

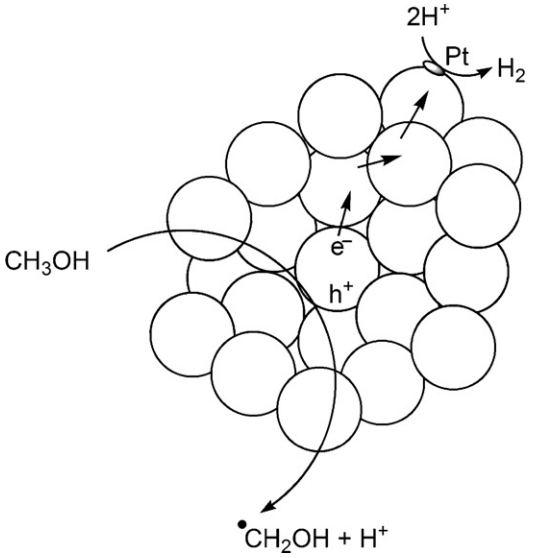

Fig. 3. Schematic illustration showing the agglomerated TiO_2 nanoparticles with an interparticle charge carrier transport leading to enhanced electron/hole pair separation and with mesoporous structure facilitating the CH_3OH diffusion through the pores.

To verify the importance of this proposed antenna mechanism, the ratio of Pt islands to TiO_2 nanoparticles has been calculated. Assuming Pt nanoparticles are spherical and have a diameter of 3.0 nm (cf. Fig. S6, supplementary data), the volume of one 3.0 nm Pt nanoparticle is calculated to be $1.41 \times 10^{-20}\,cm^3$. Considering the mass density of Pt ($21.4\,g\,cm^{-3}$), the average weight of one Pt nanoparticle is derived to be approximately 3.02×10^{-19} g. Therefore, the number of Pt islands for each gram of 0.5 wt% Pt-loaded TiO_2 will be 1.65×10^{16}. Assuming spherical TiO_2 nanoparticles with 10 nm average diameter (see Table 1) and a mass density of $3.9\,g\,cm^{-3}$, the number of TiO_2 nanoparticles per gram is calculated to be 4.91×10^{17}. Thus, the ratio of Pt islands to TiO_2 nanoparticles should be between 1 and 30. This emphasizes the importance of the transfer of the photogenerated electrons throughout the mesoporous structure.

Furthermore, the phase composition might also affect the photocatalytic activity of H_2 evolution. TiO_2 UV100 and TiO_2 P25HT consist of pure anatase phase (cf. Table S1), whereas TiO_2 P25 is a mixture of anatase and rutile (82% anatase and 18% rutile). The flat-band potential of the rutile phase coincides almost exactly with the redox potential of H^+/H_2 vs. NHE, whereas that of anatase is shifted cathodically by approximately 200 mV [31,32]. In the latter case, a considerable driving force for the proton reduction is available, while in the case of rutile this driving force will be very small. This can also explain why TiO_2 UV100 and TiO_2 P25HT are more active than TiO_2 P25.

4.2. The light intensity dependency

Fig. 2 indicates that at low light intensity ($4.40\,\mu einstein\,min^{-1}$) the rate of H_2 evolution over Pt-loaded TiO_2 P25 is similar to that observed for Pt-loaded TiO_2 UV100 and TiO_2 P25HT, whereas, at higher light intensity ($44.87\,\mu einstein\,min^{-1}$) the rate of H_2 evolution over the latter materials is about four times higher than that measured for Pt-loaded TiO_2 P25. Apparently, it is extremely important to consider the effect of light intensity when comparing different photocatalysts. A possible explanation for these differences is that the e^-/h^+ recombination rate constant is higher for Pt-loaded TiO_2 P25 leading to the fact that this undesired reaction channel becomes more significant at high light intensity in case of Pt-loaded TiO_2 P25 as compared with Pt-loaded TiO_2 UV100 and Pt-loaded TiO_2 P25HT.

It is well known that the rates of photocatalytic reactions strongly depend on both the concentration of organic compound used as test molecule and the intensity of the incident light. This behavior is usually described by an empirical kinetic expression, i.e., the so-called Langmuir–Hinshelwood rate law (Eq. (1)) [33–35].

$$R = k_r \frac{Kc}{1 + Kc} \eta (I_0)^{\beta} \quad (1)$$

where the kinetic parameters k_r and K are assumed to be independent from the incident light intensity I_0, with $\beta = 1$ at low values of I_0, and $\beta = 0.5$ at higher I_0 values. β is an empirical constant related to the ratio between interfacial charge transfer and recombination of the charge carriers. Combining the definition of the initial photonic efficiency ζ_0, i.e., the ratio between the initial H_2 production rate and the incident flux of photons I_0, with Eq. (1) for the initial concentration $c = c_0$ yields

$$\zeta_0 = k_r \frac{Kc_0}{1 + Kc_0} \eta (I_0)^{\beta - 1} \quad (2)$$

$$\log(\zeta_0) = \log\left(k_r \frac{Kc_0}{1 + Kc_0} \eta\right) + (\beta - 1)\ \log(I_0) \quad (3)$$

Eq. (2) predicts that the initial photonic efficiency ζ_0 should depend on the initial concentration of the degraded molecule c_0 as well as on the incident photon flux I_0. High concentrations of methanol were employed during the rate measurements and kept constant to ensure that the measured rate is uneffected by the methanol concentration. Plotting $\log(I_0)$ vs. $\log(\zeta_0)$ indicates a linear relation as shown in Fig. S7 (see supplementary data). According to Eq. (3), the values of β were calculated from the slopes obtained by linear regression and estimated to be 0.84, 0.83, and 0.29 for Pt-loaded TiO_2 UV100, Pt-loaded TiO_2 P25HT and Pt-loaded TiO_2 P25, respectively. A β value of 0.5 was observed in many systems as concluded from the linear dependence between the square root of the absorbed light intensity and the quantum efficiency [19,33,36–38]. Since β is an empirical constant related to the ratio between interfacial charge transfer and recombination of the charge carriers, it is very likely that the β value differs from one photocatalyst to another as experimentally found in the present study.

4.3. The methanol oxidation mechanism

According to the literature [8,12,13,19,39,40] and depending on the detected products of the photocatalytic methanol oxidation, it is concluded that methanol is photooxidized to carbon dioxide via the formation of the stable intermediates formaldehyde and formic acid (Eqs. (4)–(7)). The individual reaction steps are summarized elsewhere [20].

$$CH_3OH \xrightarrow{h\nu,\ Pt@TiO_2} CH_2O + H_2 \quad (4)$$

$$CH_2O + H_2O \rightarrow CH_2(OH)_2 \quad (5)$$

$$CH_2(OH)_2 \xrightarrow{h\nu,\ Pt@TiO_2} HCOOH + H_2 \quad (6)$$

$$HCOOH \xrightarrow{h\nu,\ Pt@TiO_2} CO_2 + H_2 \quad (7)$$

The e^-/h^+ pairs photogenerated in the TiO_2 particles upon photoexcitation will migrate to their surfaces where these redox reactions take place. The photogenerated electron will be trapped at the Pt islands followed by the reduction of a proton from water or/and from methanol producing adsorbed H• radicals. On the oxidative side, the photogenerated holes will either react with surface Ti–OH groups producing trapped holes or with adsorbed water molecules producing adsorbed •OH radicals or they will be transferred directly to adsorbed methanol molecules. However, the present study does not enable any differentiation between these pathways. The methanol photooxidation through the •OH pathway has been suggested to occur on bare titanium dioxide surfaces [12,13,19,39,40]. Regardless of which oxidation pathway is more likely, the only expected product of these reaction pathways are $^{\bullet}CH_2OH$ and $CH_3O^{\bullet}$ formed by hydrogen abstraction from the carbon atom and from the –OH group of CH_3OH, respectively. Asmus et al. [41] showed that in homogeneous aqueous solutions the efficiency of the reaction of •OH radicals with CH_3OH by hydrogen abstraction from the carbon atom is 93%. The remaining 7% is accounted for by the formation of methoxy radicals $CH_3O^{\bullet}$.

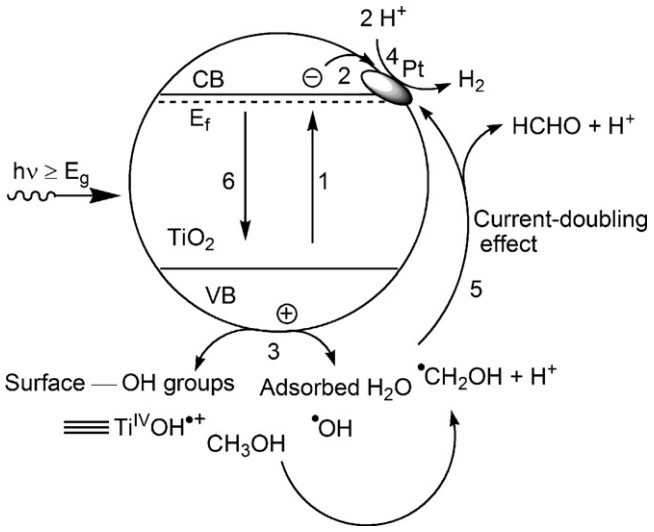

Fig. 4. Schematic representing the proposed steps for the photocatalytic molecular hydrogen production from aqueous methanol solution, (1) photogeneration of charge carriers, e^- and h^+; (2) trapping of e^- by Pt islands; (3) first oxidation step of CH_3OH either by trapped hole or by hydroxyl radical, •OH; (4) reduction of H^+; (5) formation of HCHO through e^- injection into the conduction band of TiO_2 or to the Pt islands (current-doubling); (6) recombination channel.

Methoxy radicals are subsequently reacting with methanol producing $^{\bullet}CH_2OH$ [42]. In the absence of O_2, the only way to form HCHO from $^{\bullet}CH_2OH$ is via electron injection either into the conduction band of TiO_2 or directly into the Pt islands since this radical has a reduction potential more negative than that of the conduction band of TiO_2 [8]. This dark process is referred to as "current-doubling" in photoelectro-chemistry and has been observed in many related systems including the photoanodic oxidation of alcohols on TiO_2 electrodes [43–46]. The injected electron from $^{\bullet}CH_2OH$ allows, in principle, the H_2 formation even after the absorption of just one photon. These proposed steps for the photocatalytic H_2 evolution from aqueous methanol solutions over platinized TiO_2 are schematically summarized in Fig. 4. HCHO can be further oxidized in an analogous manner producing HCOOH and finally CO_2 [47–51].

The quantitative analysis of the photocatalytic methanol oxidation products following 3 h of illumination employing 0.03 M aqueous methanol solution (2.25 mmol methanol) indicates that the yield of H_2 production is three times higher than the amount of HCHO formed even at different pH values (3.0, 7.0, and 10) (see Table 1). Moreover, the molar ratio of the evolved H_2 is about 2.0 times higher than the value calculated from the sum of all CH_3OH oxidation products. Assuming that HCHO, HCOOH, and CO_2 are the only products of the photocatalytic methanol oxidation, the sum of their concentrations should be equivalent to the concentration of evolved H_2. Since this is not observed here it has to be assumed that there are undetected products, e.g., carbonate and bicarbonate due to the high solubility of CO_2 in water. In an attempt to minimize the amount of secondary and tertiary photooxidation reaction of CH_3OH, the overall balance was tested after a short illumination time (15 min instead of 3 h). In this case, only HCHO was detected and the amount of evolved H_2 matches well the amount of HCHO formed even at different methanol concentrations and different pH values, e.g., 3.0 and 7.0 (see Table 1). Unfortunately, the exact source of the protons yielding H_2 cannot be determined from the present study, i.e., it is unclear whether H^+ originates from water or from CH_3OH. However, these results clearly indicate that methanol acts as the only hole scavenger resulting in equimolar H_2 production.

5. Conclusions

The photocatalytic H_2 production from aqueous methanol solutions over Pt-loaded commercial and home made TiO_2 photocatalysts has been extensively studied. The difference in the activity between the investigated photocatalysts is discussed depending on the physical properties, e.g., BET surface area, structure, and phase composition. The applied light intensity is shown to strongly affect the H_2 production rate depending on the e^-/h^+ recombination rate constant of the investigated photocatalyst. Following 3 h of illumination, the yield of H_2 evolved is found to be about 2.0 times higher than the value calculated from the sum of all photocatalytic methanol oxidation products (formaldehyde, formic acid, and carbon dioxide). This difference can only be explained by the presence of undetected products, e.g., carbonate and bicarbonate due to the high solubility of carbon dioxide in water. Following 15 min of illumination, only formaldehyde is detected and the amount of evolved H_2 matches very well the amount of formaldehyde formed even at different pH values and employing different methanol concentrations. These results clearly indicate that methanol acts as the only hole scavenger resulting in equimolar H_2 production. Hence, it seems more likely that this system should be described as a methanol dehydrogenation reaction when it is stopped at the first step of photocatalytic methanol oxidation (formaldehyde formation) or as a photocatalytic methanol reforming when carbon dioxide is detected but not as a real water splitting system. It is also important to mention that no O_2 was detected at any of the different applied conditions.

Acknowledgement

T.A.K. thanks the Egyptian Ministry of Higher Education for granting him a doctoral scholarship.

Appendix A. Supplementary data

Supplementary data associated with this article can be found, in the online version, at doi:10.1016/j.cattod.2010.08.012.

References

[1] J.G. Highfield, M.H. Chen, P.T. Nguyen, Z. Chen, Energy Environ. Sci. 2 (2009) 991.
[2] D.I. Kondarides, V.M. Daskalaki, A. Patsoura, X.E. Verykios, Catal. Lett. 122 (2008) 26.
[3] N. Lakshminarasimhan, E. Bae, W. Choi, J. Phys. Chem. C 111 (2007) 15244.
[4] G.L. Chiarello, L. Forni, E. Selli, Catal. Today 144 (2009) 69.
[5] G.P. Wu, T. Chen, X. Zong, H.J. Yan, G.J. Ma, X.L. Wang, Q. Xu, D.G. Wang, Z.B. Lei, C. Li, J. Catal. 253 (2008) 225.
[6] D. Bahnemann, A. Henglein, J. Lilie, L. Spanhel, J. Phys. Chem. 88 (1984) 709.
[7] D. Bahnemann, A. Henglein, L. Spanhel, Faraday Discuss. 78 (1984) 151.
[8] C.Y. Wang, R. Pagel, D.W. Bahnemann, J.K. Dohrmann, J. Phys. Chem. B 108 (2004) 14082.
[9] J. Kiwi, M. Grätzel, J. Phys. Chem. 88 (1984) 1302.
[10] P. Pichat, New J. Chem. 11 (1987) 135.
[11] A. Sclafani, M.N. Mozzanega, P. Pichat, J. Photochem. Photobiol. A – Chem. 59 (1991) 181.
[12] J. Chen, D.F. Ollis, W.H. Rulkens, H. Bruning, Water Res. 33 (1999) 661.
[13] J. Chen, D.F. Ollis, W.H. Rulkens, H. Bruning, Water Res. 33 (1999) 669.
[14] H.Q. Junwang Tang, Jinhua Ye, Chem. Mater. 19 (2007) 116–122.
[15] J. Jitputti, S. Pavasupree, Y. Suzuki, S. Yoshikawa, J. Solid State Chem. 180 (2007) 1743.
[16] S. Ekambaram, J. Alloy Compd. 448 (2008) 238.
[17] J. Jitputti, Y. Suzuki, S. Yoshikawa, Catal. Commun. 9 (2008) 1265.
[18] O. Rosseler, M.V. Shankar, M. Karkmaz-Le Du, L. Schmidlin, N. Keller, V. Keller, J. Catal. 269 (2010) 179.
[19] C.Y. Wang, J. Rabani, D.W. Bahnemann, J.K. Dohrmann, J. Photochem. Photobiol. A – Chem. 148 (2002) 169.
[20] T.A. Kandiel, R. Dillert, D.W. Bahnemann, Photochem. Photobiol. Sci. 8 (2009) 683.
[21] T.A. Kandiel, A. Feldhoff, L. Robben, R. Dillert, D.W. Bahnemann, Chem. Mater. 22 (2010) 2050.
[22] A.A. Ismail, D.W. Bahnemann, L. Robben, V. Yarovyi, M. Wark, Chem. Mater. 22 (2010) 108.
[23] T. Nash, Biochem. J. 55 (1953) 416.
[24] K. Nishijima, Y. Fujisawa, N. Murakami, T. Tsubota, T. Ohno, Appl. Catal. B – Environ. 84 (2008) 584.
[25] N. Serpone, R. Terzian, D. Lawless, P. Kennepohl, G. Sauve, J. Photochem. Photobiol. A – Chem. 73 (1993) 11.
[26] N. Serpone, A. Salinaro, Pure Appl. Chem. 71 (1999) 303.
[27] B. Ohtani, Chem. Lett. 37 (2008) 217.
[28] N. Lakshminarasimhan, W. Kim, W. Choi, J. Phys. Chem. C 112 (2008) 20451.
[29] C.Y. Wang, R. Pagel, J.K. Dohrmann, D.W. Bahnemann, C.R. Chim. 9 (2006) 761.
[30] A.A. Ismail, D.W. Bahnemann, I. Bannat, M. Wark, J. Phys. Chem. C 113 (2009) 7429.
[31] M.V. Rao, K. Rajeshwar, V.R. Paiverneker, J. Dubow, J. Phys. Chem. 84 (1980) 1987.
[32] K.E. Karakitsou, X.E. Verykios, J. Phys. Chem. 97 (1993) 1184.
[33] C. Kormann, D.W. Bahnemann, M.R. Hoffmann, Environ. Sci. Technol. 25 (1991) 494.
[34] J. Tschirch, R. Dillert, D. Bahnemann, J. Adv. Oxid. Technol. 11 (2008) 193.
[35] M.R. Hoffmann, S.T. Martin, W.Y. Choi, D.W. Bahnemann, Chem. Rev. 95 (1995) 69.
[36] L.Z. Sun, J.R. Bolton, J. Phys. Chem. 100 (1996) 4127.
[37] S. Goldstein, D. Behar, J. Rabani, J. Phys. Chem. C 112 (2008) 15134.
[38] S. Goldstein, D. Behar, J. Rabani, J. Phys. Chem. C 113 (2009) 12489.
[39] R.M. Gao, J. Stark, D.W. Bahnemann, J. Rabani, J. Photochem. Photobiol. A – Chem. 148 (2002) 387.
[40] J. Marugan, D. Hufschmidt, M.J. Lopez-Munoz, V. Selzer, D. Bahnemann, Appl. Catal. B – Environ. 62 (2006) 201.
[41] K.D. Asmus, H. Mockel, A. Henglein, J. Phys. Chem. 77 (1973) 1218.
[42] C.V. Sonntag, Free-radical-induced DNA damage and its repair. A chemical perspective, Springer-Verlag, Berlin, Heidelberg, New York, 2006.
[43] N. Hykaway, W.M. Sears, H. Morisaki, S.R. Morrison, J. Phys. Chem. 90 (1986) 6663.
[44] Y. Nosaka, H. Sasaki, K. Norimatsu, H. Miyama, Chem. Phys. Lett. 105 (1984) 456.
[45] G. Nogami, J.H. Kennedy, J. Electrochem. Soc. 136 (1989) 2583.
[46] R. Memming, Top. Curr. Chem. 169 (1994) 105.
[47] L.D. Burke, W.A. Oleary, J. Electrochem. Soc. 135 (1988) 1965.
[48] W.Y. Teoh, L. Madler, R. Amal, J. Catal. 251 (2007) 271.
[49] T.L. Villarreal, R. Gomez, M. Neumann-Spallart, N. Alonso-Vante, P. Salvador, J. Phys. Chem. B 108 (2004) 15172.
[50] P. Herrasti, L. Peter, J. Electroanal. Chem. 305 (1991) 241.
[51] Y. Maeda, A. Fujishima, K. Honda, J. Electrochem. Soc. 128 (1981) 1731.